USE OF ARTIFICIAL INTELLIGENCE METHODS IN SELECTION OF VARIABLE TENSION PULLEY DIAMETER IN BELT PULLEY MECHANISMS

Serkan Beller

Department of Natural Gas and Fitting Technology, Vocational School of İmamoğlu, Çukurova University, Adana 01790, Turkey

Abstract

Belt pulley systems transfer power and motion from shaft to shaft via a flexible, bendable belt wrapped around pulleys. The flexibility and bendability of the belt prevent the negative effects, such as vibration and impact, that may occur on one shaft from being transferred to the other shaft. Power transmission occurs through the friction (force) bond between the belt and the pulley. There may be slippage between the belt and the pulley during moment increases. While this provides an advantage in that sudden load increases are not transmitted to the motor shaft, it provides a disadvantage in that it does not provide a constant rotation ratio. Another disadvantage of these mechanisms is the occurrence of permanent belt elongation over time, and tensioning systems are needed to eliminate the looseness. In addition to these disadvantages, the shaft bearings are strained due to the forces exerted by the arms pressing the belt against the pulley, and the power transmission is limited by the belt's strength. In this study, a group of pulleys consisting of different diameters was used as a tension pulley as an alternative to weighted or spring tension pulleys. Different weights that have different distances from the main pulley (Driven pulley) hub were tested with different rotation speeds and tension pulleys with different diameters in the experimental set. In addition, the number of revolutions of the main pulley was also estimated using artificial intelligence methods. Thus, by ensuring minimum slippage with the most suitable tension pulley diameter, an attempt was made to prevent possible strain on the shaft bearing and belt.

Keywords: *belt pulley mechanisms, tension pulley, artificial intelligence, GRNN, ANFIS*

1. INTRODUCTION

Belt and pulley mechanisms transmit power and energy between machines and other structures. Thanks to these mechanisms, communication is provided between elements and machines that have large gaps between them or are not in the same environment. Belts are wrapped around pulleys mounted on the driving or driven conveying elements. The transmission of force between the belt and pulley in flat, trapezoidal, and round forms is achieved through friction bond, and in toothed belts, through shape bond. The formation of friction bonds in flat and trapezoidal belts is achieved by giving sufficient tension force to the belt. This creates an additional radial load on the shaft and bearings, depending on the magnitude of the transmitted torque [1].

The advantages of belt mechanisms are as follows. Firstly, since the belts are made of elastic materials such as rubber, their ability to absorb impacts is good. In joining finite belts, they operate quietly if noise at the joint can be prevented. Except for the toothed belts, they are cheap because their structure is simple and easy to produce. They can transmit force and motion at large axial distances. The distance is not directly dependent on the pulley diameters. They do not transmit pulsed or instantaneous load changes, so they work as a safety element for the system. The rotation ratio can be easily adjusted by simply changing the pulley diameter. With cross winding, the direction of the moment can be changed, and in transmission shafts, more than one shaft can be driven with a single belt. The disadvantages of belt mechanisms are as follows: First of all, they take up more space than gear mechanisms. Since the moment is transmitted by friction, large bearing forces can occur. Except for toothed belts, since partial slip (1%-2%) occurs in the motion transmission. A full and constant conversion ratio cannot be ensured. Due to the belt elongation and wear on the belt over time, a mechanism that changes the shaft axis distance or tension pulley mechanisms is needed. The flexibility and internal structure of the belt change over time with temperature and humidity, and the coefficient of friction between the belt and the pulley is affected by operating conditions (dust, humidity, etc.) [2]. For the belt-pulley mechanisms, power can

be transmitted if the friction force (F_s) between the belt and the pulley is the same or greater than the transmitted force (F_t). This way, the belt system can be kept under control. The centrifugal force (F_{mk}), which increases with the rotation speed of the belt, causes the belt to elongate. It also reduces the pressure force and transmission power of the pulley in an undesirable way. To reduce its effect, special measures such as idler pulleys, automatic mechanisms, etc., are used [1].

In the study [3], a smart transmission system (a triboelectric V-belt (TVB)) was proposed. Slipping failure of the V-belt drive at the driven pulley can be detected in time by analyzing the amplitude and time-frequency characteristics of the TVB output current. The paper [4] introduces a new changeable radius pulley that passively changes the effective radius of the drive pulley in response to the change in load torque in a belt-driven transmission. In the article [5], an improved neural control structure is proposed to adjust the gear ratios of a CVT transmission. In [6], transient CVT shift behavior was studied. Adaptive control laws for partial linearization were suggested. The use of neural networks for identification and compensation allowed for advanced ratio control while also enabling shift rate prediction. In the study numbered [7], a systematic review was made for the dynamic modeling, simulation, and experimental studies of power transmission belt drives. As a result of the investigations, it was seen that the noise and vibration sources in belt drives are caused by the transverse vibrations of the belt spans, the rotational vibrations of the pulleys, and the belt slipping and friction on the pulleys [8–13]. In addition, sliding wear caused by friction between the belt and the pulley is also caused by dynamic stress transitions from tight to loose clearance and vice versa during work. Besides using tension pulleys, other devices, such as one-way clutches, have also been adopted in some automotive belt drives to decrease system vibrations [14,15,16]. For example, adding a rigid coupling and a spring isolator between the accessory and the pulley [14].

Ref.	Belt Type	Work. Meth.	Purpose
[3]	V Belt	Experimental	With the designed TVB, the slipping malfunction of the V-belt drive can be identified in time.
[4]	Cable	Experimental and Simulation	Explaining the operational principle of the variable radius pulley and realizing robot joint position control.
[5]	Steel Structure Belt (CVT)	Simulation	It demonstrated the reduced control fluctuations and enhanced instantaneous learning and control capacity of the improved neural control algorithm (MCMAC-ATO) for adjusting the CVT gear ratio.
[6]	Chain Driven Belt (CVT)	Simulation	Since the input-output behavior of chain-driven CVTs is nonlinear, a PI control utilizing GRNN is developed for improved ratio control and gear shift speed prediction.
[14]	V Belt	Simulation	The use of an isolator or spreader isolator (Occurrence of a one-way clutch and torsional spring) within the practical operating range of engine speeds has significantly reduced the problem of belt slippage due to dynamic tension drop across the accessory pulley.
[15]	Multi-Wedge Belt (V Belt)	Experimental and Numerical Simulation	The impact of the one-way clutch on reducing belt resonance in the belt drive system is illustrated.
[16]	Multi-Wedge Belt (V Belt)	Experimental and Simulation	Dynamic analysis of the automotive serpentine belt drive system with an automatic belt tensioner was performed.

Table 1. Previous studies.

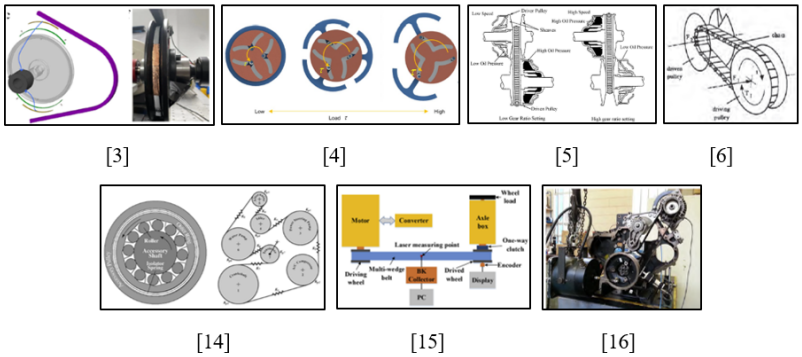

Fig. 1. Experiment sets for the previous studies.

When looking at Table 1 and Figure 1, it is seen that work is mostly done on main pulleys with V belts and CVT belts. As for the working method, experimental studies were mostly conducted on V-belt structures. Artificial intelligence methods were mostly preferred in determining gear ratios. In the current study, experiments were carried out with a round belt structure. In the studies, the focus was more on the tension pulley rather than the main pulleys. Tests were carried out with tension pulleys of different diameters at different rotation speeds, different load amounts, and different load distances to obtain the most suitable belt tension. The aim here is to select the most suitable tension pulley diameter to prevent belt slippage and unnecessary belt wear. Artificial intelligence methods were used for this, too.

Other sections of the paper are as follows. In Section 2, torque and error calculations and artificial intelligence methods are given. In Section 3, the graphical conclusions are shown. In Section 4, the discussion and conclusions are given.

2. MATERIAL AND METHOD

In the belt-pulley mechanism, the belt must be pressed onto the pulley for the transmission of movement. If the distance between the shaft axes does not change, in long belts, the belt presses the pulley with its weight, or the length of the belt is selected to be shorter than the distance between the shaft axes, and the elastic belt is extended and passed to the pulley. However, this application is possible on inclined and vertical shaft axes below five meters. Air humidity and temperature cause the properties of the belt material to change frequently. If the belt arms become loose during operation, the tension force can't remain constant. For this reason, tensioning devices are needed in belt and pulley mechanisms. In principle, tensioning devices are divided into three groups: sliding, jointed, and tension pulley systems [1]. In the current study, the tension pulley mechanism method was used. In this mechanism, instead of weights or springs, pulleys of different diameters are placed as a group on the slack arm of the belt. Belts can be passed between these pulleys with a mechanism. The belt type used in the current experimental set is round. For this purpose, a 2 mm diameter o-ring seal was used. The main pulley (Driven pulley) has a diameter of 50 mm, and the motor pulley (Driving pulley) has a diameter of 20 mm. The tension pulley diameters used for training are 0, 6, 11, 15, 18, and 30 mm, respectively. The tension pulley diameters used for testing are 13, 17, and 25 mm, respectively. All pulleys are made of hard plastic. Masses of different weights (0, 5, 12, 25, 34, 48 g for training, 4, 8.5, 20, 30, 41 g for testing) attached to the main pulley were tested for a five-second experimental period. Here, while the weight amounts were changed, the distances of the weights to the main pulley hub center were also changed (For training: 0, 22, and 38 mm, and for testing: 31 mm). During the training phase, the DC motor was rotated at seven different speeds (Analog values for training: 0.8, 1.2, 1.6, 2.0, 2.4, 2.8, 3.2), while during the testing phase, tests were performed at six different speeds (Analog values for testing: 1.0, 1.4, 1.8, 2.2, 2.6, 3.0). As a result, different rotation numbers were obtained in the main pulley in case of variable conditions. According to the experimental results, the pulley slip rates are less than seven per thousand (0.7 %). In this study, two different artificial intelligence methods from machine learning were used to predict the

results. Then, these two methods were compared with each other. One of these artificial intelligence methods is GRNN (General Regression Neural Network), and the other is ANFIS (Adaptive Network Based Fuzzy Inference System). In these network structures, 462 rows of data were utilized as training data, and 90 rows of data were used as test data. The test data have not been previously presented to the networks. Thanks to the control block developed in the MATLAB/Simulink environment, it is possible to estimate with low error which tension pulley diameter can allow how much rotation in the main pulley (Driven pulley) at different weight amounts, different distances, and different motor speeds.

2.1. Force and Moment Calculation in Belts

In belt and pulley mechanisms, motion transmission is through friction. Due to pre-tensioning, the friction force that will occur between the belt and the pulley must be greater than the moment to be transmitted. From the force balance given in Figure 2 [2],

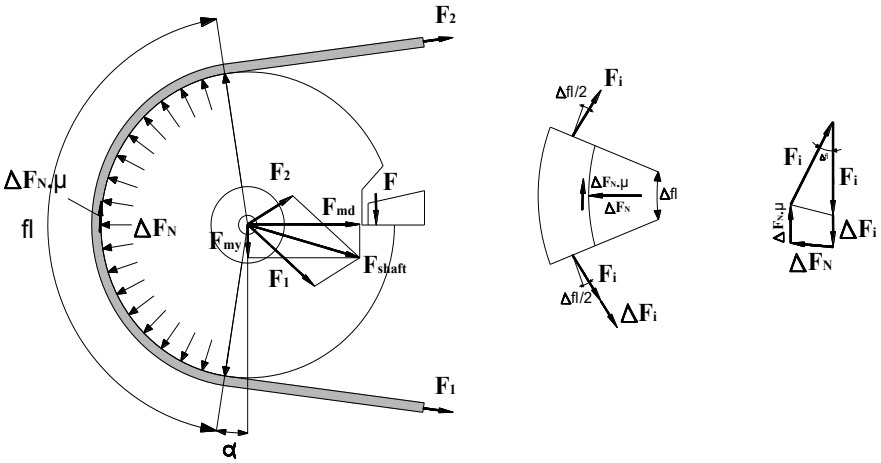

Fig. 2. Forces occurring in the belt arms.

$$\Delta F_{\dot{I}} = \Delta F_N.\mu,\ \Delta F_N = F_{\dot{I}}.\Delta\beta,\ \ \Delta F_{\dot{I}} = F_{\dot{I}}.\Delta\beta.\mu \tag{1}$$

$$\frac{\Delta F_{\dot{I}}}{F_{\dot{I}}} = \Delta\beta.\mu,\ \sum\frac{\Delta F_{\dot{I}}}{F_{\dot{I}}} = \sum(\Delta\beta.\mu) \tag{2}$$

If the integral is taken,

$$\ln F_1 - \ln F_2 = \ln\frac{F_1}{F_2} = \mu.\beta \tag{3}$$

$$\frac{F_1}{F_2} = e^{\mu\beta} \tag{4}$$

$$\frac{F_1}{F_2} = e^{\frac{\mu\pi\beta^\circ}{180}},\ m = e^{\frac{\mu\pi\beta^\circ}{180}},\ F_1 = F_2.m \tag{5}$$

$$F = F_1 - F_2,\ k = \frac{F}{F_1} = \frac{m-1}{m} \tag{6}$$

From the moment balance;

$$M_d = F.r = (F_1 - F_2).r \tag{7}$$

The belt arm forces (F_1 and F_2) are found from the common solution of (4) and (7).

Forces acting on the shaft;

If the belt arms are parallel $(i_{12} = 1)$,

$$F_{shaft} = F_1 + F_2 \tag{8}$$

If the belt arms are not parallel,

$$F_{shaft} = \sqrt{F_1^2 + F_2^2 - 2.F_1.F_2 \cos\beta} \tag{9}$$

The vertical and horizontal components of the shaft force are,

$$F_{md} = (F_1 + F_2).\cos\alpha \tag{10}$$

$$F_{my} = (F_1 - F_2).\sin\alpha \tag{11}$$

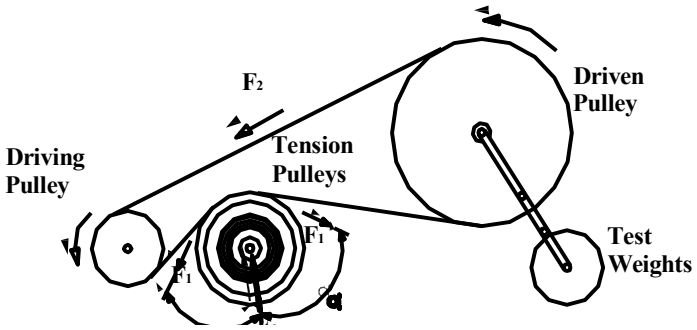

Fig. 3. Tension pulley group usage.

Placing a tension pulley, with or without a weight (spring), on the loose arm of the belt is an effective method used in belt pulley systems. In Figure 3, since the tension pulley can rotate freely, the arm forces on both sides can be considered equal (F_1) [17]. In this case, the force (F_3) of pressing the pulley onto the belt is,

$$F_3 = 2F_1.\mathrm{Cos}\,\alpha \tag{12}$$

A spring or counterweight is usually used to create this force. Here, a tension pulley group of different diameters was used.

2.2. General Regression Neural Network (GRNN)

A general regression neural network is a model utilized for system modeling and predictive analysis based on parameter dependencies. It was introduced by Donald F. Specht in 1991. In this network architecture, the learning process is rapid and can be efficiently utilized with a limited amount of data. The GRNN architecture is a feedforward network framework based on the probability density function.

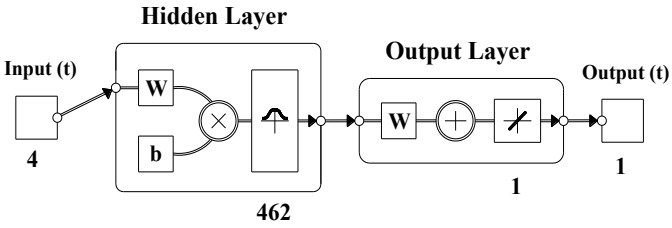

Fig. 4. GRNN representation in Matlab.

This network structure consists of four layers. The number of input neurons, similar to other networks, is determined by the number of inputs in the problem. The number of neurons in the intermediate layer matches the number of samples. The neurons in the summation layer are one more than the number of outputs [18]. Figure 4 shows the general appearance of GRNN in MATLAB. During programming, the user selects a *spread* parameter. A broader *spread* means creating more space around the input vector. The *spread* value should be set between 0 and 1 for optimal performance. The smaller the number, the better the best-fit approximation. The higher the value, the smoother the approximation performance (Sahroni, 2013) [19].

2.3. Adaptive Network-Based Fuzzy Inference System (ANFIS)

In 1993, Jang suggested the ANFIS method. This algorithm occupies a special place in graded learning. The most widely applied graded inference method in ANFIS is the Takagi-Sugeno-Kang graded inference system (Takagi and Sugeno, 1985; Sugeno and Kang, 1986) [20]. The parameters of ANFIS have been refined within the scope of the adaptive neural network. An adaptive network is a network framework consisting of nodes and the connections linking these nodes [20]. Contemporary neuro-fuzzy systems are typically feedforward and multilayered. The ANFIS model incorporates a fuzzy system, such as Sugeno, and utilizes backpropagation learning [21]. Figure 5 shows the general view of ANFIS. While training these network structures, a "fuzzy" neural network toolbox was preferred in MATLAB/Simulink. The epoch value was 5000 in all trials, and the goal was 0.

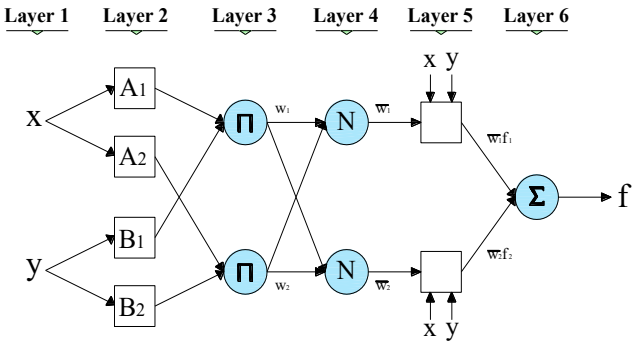

Fig. 5. ANFIS general view.

2.4. System Design

In this study, Pololu 12 V brushed geared DC motor (2250 RPM, 48 CPR quadrature encoder) [22], Pololu motor controller card 24V23A [23], Humusoft MF 634 DAQ card [24], Encoder Omron E6A2 CW3C [25], power supply (12 V, 16.7 A), and a computer (Windows 7, 64 bit, Intel Core i5-7500, 3.40 GHz, 16 GB RAM) were used.

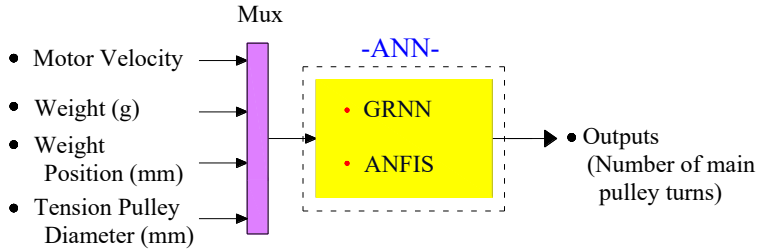

Fig. 6. Control block.

As shown in Figure 6, studies were conducted on this control block in the MATLAB/Simulink environment. Four distinct datasets were utilized as input. The first is the analog value for the DC motor speed; the second is the test weight value; the third is the distance of the test weight to the center of the main pulley shaft, and the fourth is the value of the tension pulley diameter. The output data is the number of main pulley rotations. Firstly, the GRNN network structure was tested in the control block. Then, the ANFIS network structure was tested. The success rates of these two networks are shown in the results section.

2.5. Calculation of Error Values

Performance evaluations of training and test results were realized with Root Mean Square Error (RMSE), Regression Coefficient (R^2), and Mean Absolute Error (MAE) values. They were determined in Excel with the help of equations 14, 15, and 16, respectively.

A_j = Actual values, P_j = Predicted values, n = Size of the data set, e_j =Error

$$e_j = A_j - P_j \tag{13}$$

Root Mean Square Error (RMSE) [26], best value = 0, worst value = +∞

$$RMSE = \sqrt{\frac{1}{n}\sum_{t=1}^{n} e_j^2} \tag{14}$$

Regression Coefficient (R^2) [27], best value = +1, worst value = -∞

TSS = Total Sum of Squares, RSS = Residual Sum of Squares

$$R^2 = \frac{TSS - RSS}{TSS} \tag{15}$$

Mean Absolute Error (MAE) [28], best value = 0, worst value = +∞

$$MAE = \frac{1}{n}\sum_{t=1}^{n} \left| e_j \right| \tag{16}$$

MSE denotes the mean of the squared differences between actual and predicted values. It measures the variance of the residuals. RMSE is the square root of MSE. Measures the standard deviation of the residuals. The measure of the agreement between the true value and the model's prediction is R^2. It is found by dividing the actual values' variance by the estimated values' variance. This situation expresses how well or not the model fits. MAE signifies the average of absolute differences between the predicted and actual values. It quantifies the average magnitude of residuals in the dataset.

3. RESULTS

In this study, machine learning methods GRNN and ANFIS were preferred. According to Table 2, four different types of input data were used, while one output data set was obtained for these networks in the training and testing stages. In these network structures, 462 rows of data were utilized as training data,

and 90 rows of data were used as test data. The test data have not been previously presented to the networks.

	Training Data	**Test Data**
Motor Velocity	0.8, 1.2, 1.6, 2.0, 2.4, 2.8, 3.2	1.0, 1.4, 1.8, 2.2, 2.6, 3.0
Weight (g)	0, 5, 12, 25, 34, 48	4, 8.5, 20, 30, 41
Weight Position (mm)	0, 22, 38	31
Tension Pulley Diameter (mm)	0, 6, 11, 15, 18, 30	13, 17, 25

Table 2. Training and test data.

The measurement parameters of the relevant experimental setup are presented in Figure 7. The success rates of the networks were interpreted with the results of RMSE, R^2, and MAE. Consequently, an assessment will be conducted to determine how closely artificial intelligence techniques can match the true experimental outcomes, considering these error margins. The success rates of the networks were determined by the fact that the R^2 results were close to 1, while the RMSE and MAE results were near 0.

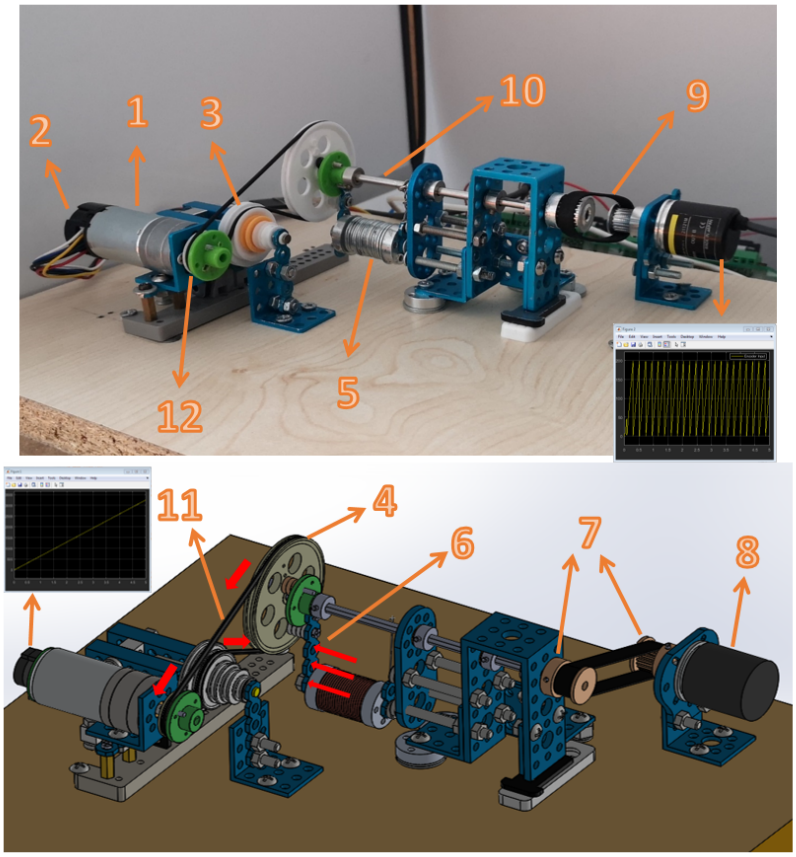

Fig. 7. Experiment set: 1. DC motor, 2. DC motor's encoder, 3. Tension pulley group, 4. Main pulley (θ 50 mm), 5. Test weights, 6. Three different weight positions (22, 31, and 38 mm), 7. Main shaft gear pulley (θ 10 mm) and encoder gear pulley (θ 10 mm), 8. The encoder of the main shaft, 9. Encoder gear belt, 10. Main shaft (θ 4 mm), 11. Load belt (θ 2 mm), 12. DC motor pulley (θ 20 mm).

During the study, various analog signal values were chosen to operate the DC motor at diverse speeds. The values of these signals, such as tangential velocity (m/s) and RPM on the DC motor shaft (No-load), are represented in Figure 8. In this study, the DC motor's speed capacity was set to 100% percent.

When Table 2 is examined, it is seen that seven different speeds were used for motor speeds during training. The training was conducted with six different weight values and three different distances as positions. In addition, training was conducted with six different diameter pulleys as tension pulleys. On the other hand, the tests were conducted with six different motor speeds, five different weights, and one different distance value as positions. In addition, tests were conducted with three different diameter pulleys as tension pulleys. Thus, 462 lines of data were obtained as training data, and 90 lines of data were obtained as test data.

While creating the training data, tension pulleys of six different diameters were used. The diameters of these pulleys are 0, 6, 11, 15, 18, and 30 mm. Only those with diameters of 18 mm and 30 mm were able to rotate the main pulley. These rotation amounts are seen in Figure 10 in the training and test results section. While creating the test data, tension pulleys of three different diameters were used. The diameters of these pulleys are 13, 17, and 25 mm. Only tension pulleys with diameters of 17 mm and 25 mm were able to rotate the main pulley. These rotation amounts are seen in Figure 11 in the training and test results section.

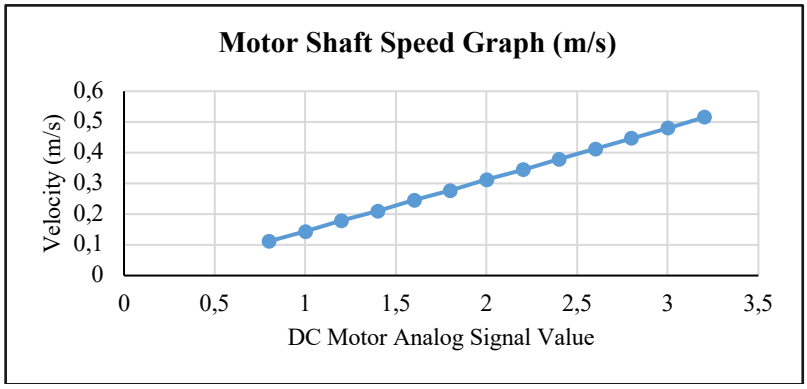

a)

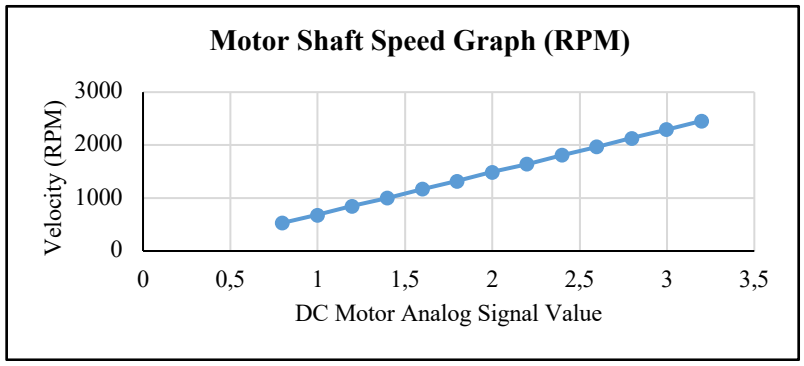

b)

Fig. 8. Motor shaft analog signal-velocity graphs. a) (m/s), b) (RPM)

3.1. GRNN Experiment Results

This study tested eight different *spread* values (0.000001, 0.00001, 0.0001, 0.001, 0.01, 0.1, 1, and 10) to determine the optimal performance. As represented in Table 3, it can be observed that the training and test results remain unchanged for values where the *spread* value is 0.01 or lower, up to four decimal places. The 'Train R^2' result is one, the 'Train RMSE' result is zero, and the 'Train MAE' result is zero at

the first five *spread* values. Therefore, the optimal performance was determined with a *spread* value of 0.01.

Spread	0.000001	0.00001	0.0001	0.001	**0.01**	0.1	1	10
Train. R^2	1	1	1	1	**1**	1	0.9650	0.7949
Test. R^2	0.9995	0.9995	0.9995	0.9995	**0.9995**	0.9995	0.9673	0.8064
Train. RMSE	0	0	0	0	**0**	0.0067	642.69	1990.39
Test. RMSE	122.13	122.13	122.13	122.13	**122.13**	122.13	749.49	3404.06
Train. MAE	0	0	0	0	**0**	0.0017	219.58	900.42
Test. MAE	57.66	57.66	57.66	57.66	**57.66**	57.66	367.06	1997.64

Table 3. The performance results of *spread* values for GRNN.

3.2. ANFIS Experiment Results

In this study, eight membership function (MF) types have been tried as seen in Table 4. Values of input set numbers (MFs) are determined as 2222, 3333. In all studies, the fault tolerance was determined as 0, and the epoch value was 5000. The results are presented in Table 5. The closer the results of R^2 to 1, and the closer to 0 the results of RMSE, and MAE, the higher the success. The successful results were obtained in the 15th-row and 16th-row ANFIS structures. The network in row 15 is the most successful because the fifth and sixth digits after the decimal point, and the subsequent digits, have lower values in that network structure.

	Network Type	**Membership Fuction**	**Input Set Numbers**	**Error Tolerance**	**Epochs**
1	ANFIS	*trimf*	2222	0	5000
2	ANFIS	*trapmf*	2222	0	5000
3	ANFIS	*gbellmf*	2222	0	5000
4	ANFIS	*gaussmf*	2222	0	5000
5	ANFIS	*gauss2mf*	2222	0	5000
6	ANFIS	*pimf*	2222	0	5000
7	ANFIS	*dsigmf*	2222	0	5000
8	ANFIS	*psigmf*	2222	0	5000
9	ANFIS	*trimf*	3333	0	5000
10	ANFIS	*trapmf*	3333	0	5000
11	ANFIS	*gbellmf*	3333	0	5000
12	ANFIS	*gaussmf*	3333	0	5000
13	ANFIS	*gauss2mf*	3333	0	5000
14	ANFIS	*pimf*	3333	0	5000
15	**ANFIS**	***dsigmf***	**3333**	**0**	**5000**
16	ANFIS	*psigmf*	3333	0	5000

Table 4. ANFIS training features.

	Train. R^2	Test R^2	Train. RMSE	Test RMSE	Train. MAE	Test MAE
1	0.9995	0.9994	74.076	2751.7	20.241	1482.5
2	0.9994	0.9996	78.443	605.92	21.946	320.82
3	0.9994	0.9996	76.463	2625.8	27.600	1422.9
4	0.9994	0.9995	75.744	3401.7	21.217	1834.5
5	0.9995	0.9997	74.375	355.98	19.899	185.70
6	0.9919	0.9787	298.62	745.72	136.64	351.25
7	0.9477	0.9451	760.66	1983.3	536.78	1351.5
8	0.9480	0.9452	758.59	1993.0	534.73	1356.0
9	0.9995	0.9993	67.339	1751.9	16.441	940.79
10	0.9995	0.9989	69.306	347.83	17.103	172.40
11	0.9995	0.9993	70.214	959.69	29.089	520.38
12	0.9996	0.9993	65.332	2552.7	15.082	1374.2
13	0.9995	0.9990	69.948	374.10	25.349	199.49
14	0.9995	0.9905	68.487	419.24	18.300	208.60
15	**0.999568**	**0.996339**	**69.136858**	**333.800840**	**22.512265**	**167.465849**
16	0.999568	0.996339	69.136859	333.800889	22.512269	167.465881

Table 5. ANFIS training results.

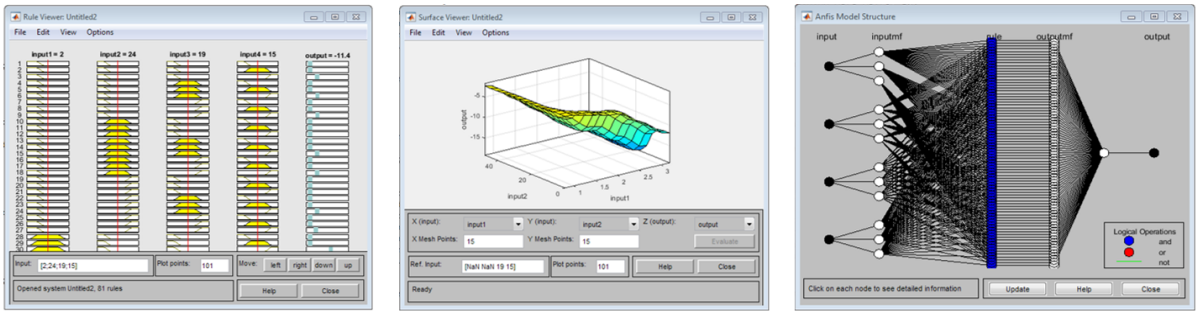

Fig. 9. Rule viewer, surface viewer, and model structure for 15th row ANFIS structure.

ANFIS training was finished at epoch 2. The data of the network are as follows: quantity of nodes: 193, quantity of linear parameters: 81, quantity of nonlinear parameters: 48, total number of parameters: 129, quantity of training data pairs: 462, quantity of checking data pairs: 0, quantity of fuzzy rules: 81. Also, Figure 9 shows the rules, surface, and model structures. A total of 462 lines (83.69 %) of data were used for training and 90 lines (16.30 %) for testing. The total number of data is 552 rows. Test data has never been introduced to the network before.

3.3. Training and Test Results

As seen in Figure 10, rotations were achieved in the main pulley when only tension pulleys with diameters of 18 and 30 mm were used in the training data. Since tension pulleys with diameters of 0, 6,

11, and 15 mm could not provide rotation in the main pulley, they were not presented graphically. Figure 10-a shows the results for seventy-seven experiments conducted under different conditions when using an 18 mm tension pulley. The number of motor pulley rotations ranges from 42.1 to 203.37. In the same graph, the main pulley rotation count varies between 0.01 and 0.160. Looking at Figure 10-b for the 30 mm tension pulley, it can be seen that the motor pulley rotation values vary between 38.64 and 201.25. The main pulley rotation values, on the other hand, vary between 10.38 and 68.79. According to the graphical results, it is observed that as the diameter of the tension pulley increases, the rotational speed of the main pulley also increases.

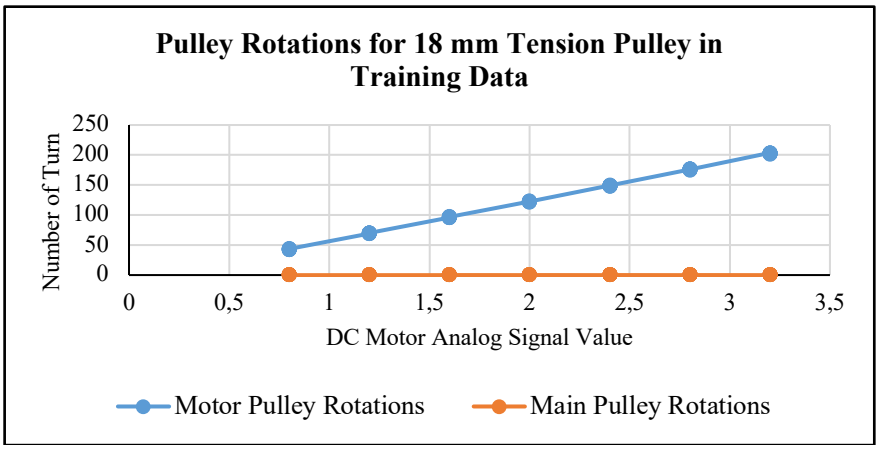

a)

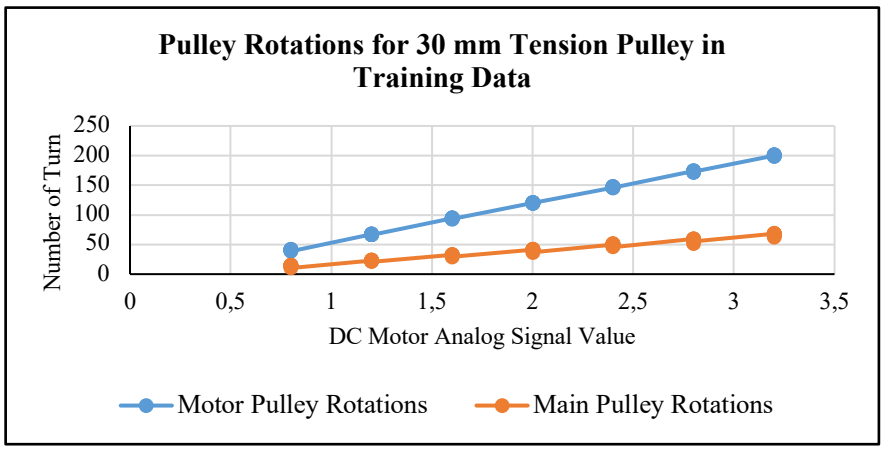

b)

Fig. 10. Pulley rotations in training data: a) For 18 mm tension pulley, b) For 30 mm tension pulley.

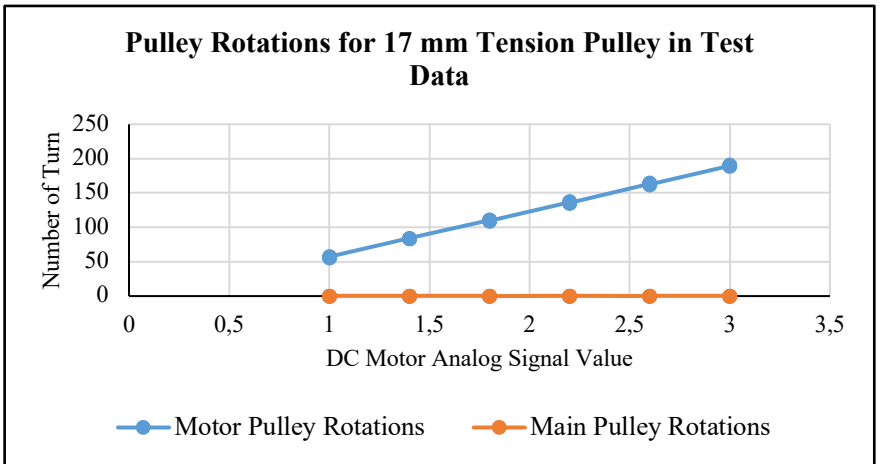

a)

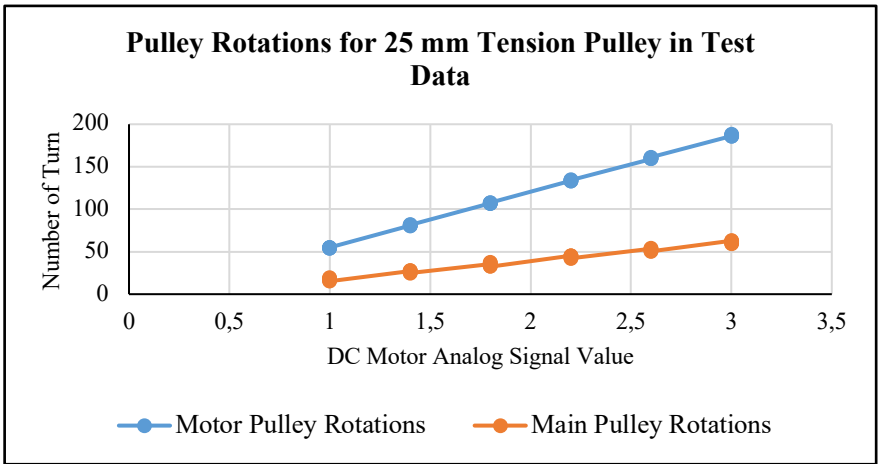

b)

Fig. 11. Pulley rotations in test data: a) For 17 mm tension pulley, b) For 25 mm tension pulley.

When looking at Figure 11, rotations were achieved in the main pulley only when tension pulleys with diameters of 17 and 25 mm were used in the test data. Since the tension pulley with a diameter of 13 mm could not provide rotation in the main pulley, it was not presented graphically. Figure 11-a shows the results for thirty experiments conducted under different conditions when using a 17 mm tension pulley. The number of motor pulley rotations ranges from 56.02 to 191.14. In the same graph, the main pulley rotation count varies between 0.01 and 0.125. Looking at Figure 11-b for the 25 mm tension pulley, it can be seen that the motor pulley rotation values vary between 53.75 and 188.04. The main pulley rotation values, on the other hand, vary between 15.28 and 62.87. As the diameter of the tension pulley increases, the number of revolutions of the main pulley also increases. During training and tests, the amount of weight carried, as well as the speed of the DC motor and the distance between the centers of gravity of the weights and the main pulley hub, are constantly increasing.

3.4. Comparison of Experiment Results

In the present study, two distinct artificial intelligence techniques from machine learning methods were used. As shown in Table 6, the GRNN method produced the best results. In the 5% error rate evaluation, 100% success was attained in the training data, and 77.78% success was attained in the test data. On the other hand, in the 10% error rate evaluation, 100% success was attained in the training data, and 87.78% success was attained in the test data. In the test data, the most challenging task for the neural networks is estimating the number of main pulley turns using a 17 mm diameter tension pulley. In tension pulley tests with this diameter, the main pulley never completed a full turn. This makes network predictions

difficult. When using a tension pulley with a diameter of 25 mm, the main pulley turn number estimation rate is much higher. The highest success rate was achieved when a tension pulley with a diameter of 13 mm was used. Because the number of the main pulley turns is zero.

	Network Type	Train Data for 0%, 5%, and 10% Error	Test Data for 0%, 5%, and 10% Error	Train R^2	Test R^2	Train RMSE	Test RMSE	Train MAE	Test MAE
1	**GRNN**	**100 %**	**46.67 %**						
		100 %	**77.78 %**	**1**	**0.9995**	**0**	**122.13**	**0**	**57.66**
		100 %	**87.78 %**						
2	ANFIS	0 **%**	0 **%**						
		16.67 **%**	14.44 **%**	0.9995	0.9963	69.136	333.80	22.512	167.46
		17.96 **%**	25.56 **%**						

Table 6. Comparison of the networks' performance results.

When the ANFIS network structure is examined, it is shown that the test RMSE values and test MAE values are almost three times worse than those of GRNN. The 5% and 10% error rates are also well below the expected. In the 5% error rate evaluation, 16.67% success was attained in the training data, while 14.44% success was attained in the test data. In the 10% error rate evaluation, 17.96% success was attained in the training data, while only 25.56% success was attained in the test data. The following method was used to calculate the percentage success rates: First, two absolute formulas were written in Excel according to tolerance ranges of 5% and 10%.

A = Measured Value, B = Desired Value.

If A > B + 0.05B or A < B - 0.05B = 0 (It was deemed a failure.) (17)

If A ≤ B + 0.05B and A ≥ B - 0.05B = 1 (It was deemed successful.) (18)

$\text{Total Number of Correct Answers} = \Sigma x$, $\text{Total Number of False Answers} = \Sigma y$;

$\Sigma 1 = \Sigma x$, $\Sigma 0 = \Sigma y$

These formulas were applied to each experimental result. All results falling within these tolerance ranges were counted and then summed. This yielded the number of correct and incorrect answers for each network. The values 0 and 1 were used as binary indicators. The aim here was to easily count the total number of correct and incorrect answers. Then, the percentage success rates of the networks were determined by applying the following formulas.

$$\%Success\ Rate = \frac{\Sigma x}{\Sigma(x+y)}.100 \text{ for the correct answers.} \quad (19)$$

$$\%Success\ Rate = \frac{\Sigma y}{\Sigma(x+y)}.100 \text{ for the false answers.} \quad (20)$$

3.5. Amount of Slip

Figure 12 shows an example of the main pulley encoder results obtained during training. The graph shows two distances labeled A and B.

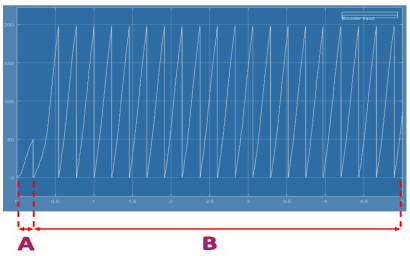

Fig. 12. Main pulley encoder measurement. (1.2-48g-38mm-30mm Pulley Diameter)

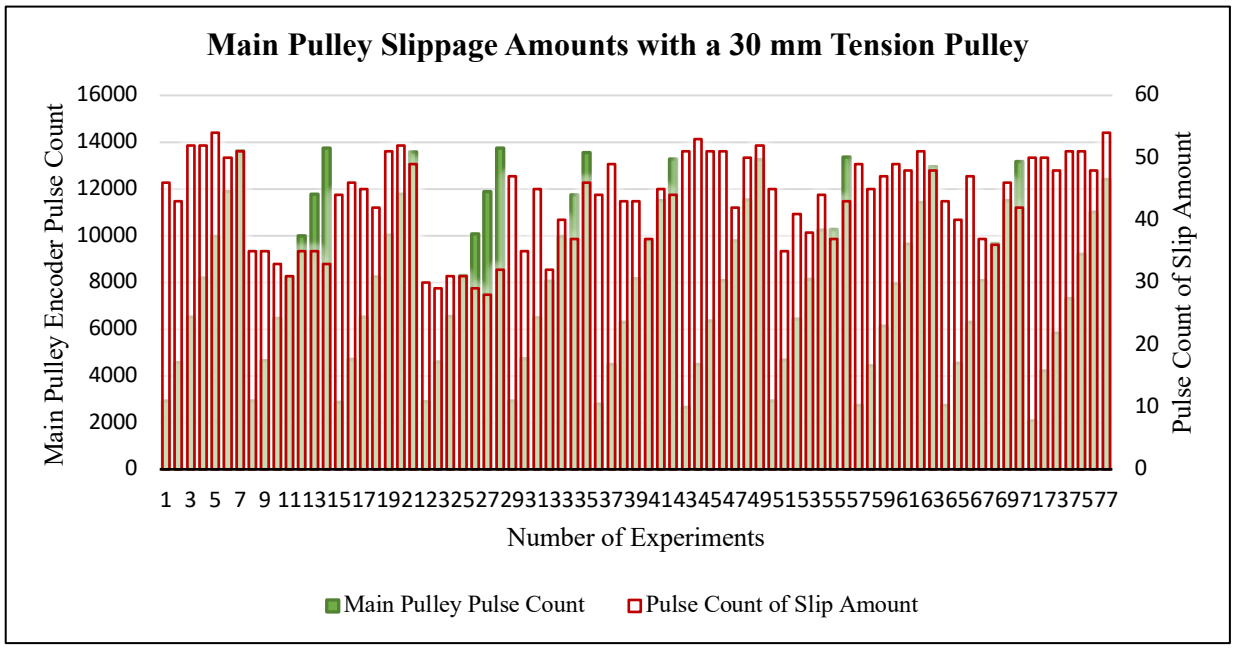

a)

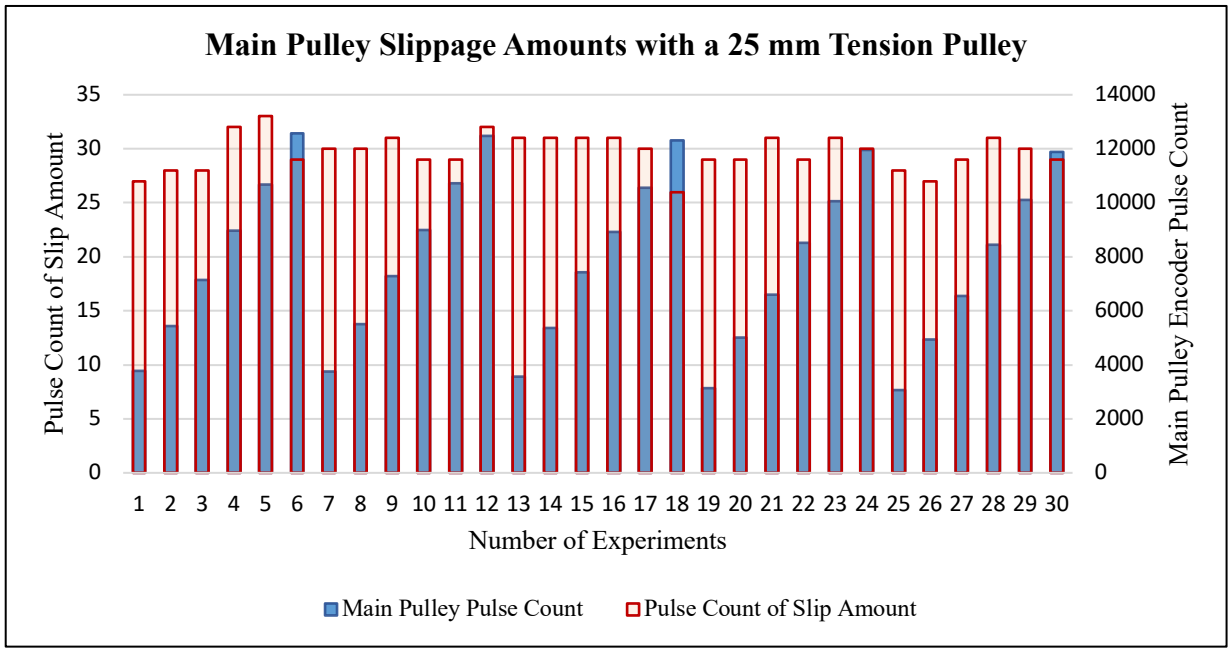

b)

Fig. 13. Pulse values of main pulley slip amount. a) Training data, b) Test data.

Distance A indicates both the duration and the pulse value of the slip amount obtained when the movement is first started. Distance B shows the duration and pulse values of the remaining movement over a period of five seconds. These slippage amounts were observed only when working with a 30 mm tension pulley diameter for the training data. No slippage occurred while operating with an 18 mm diameter tensioning pulley. In the test data, this amount of slippage was observed only when operating with a tensioning pulley diameter of 25 mm. No slippage occurred while operating with a 17 mm diameter tensioning pulley. In the training data, only seventy-seven experiments were conducted with a 30 mm tensioning pulley diameter. In the test data, only thirty experiments were conducted with a 25 mm tensioning pulley diameter. The average slippage value for the training data was obtained as 0.699%. For the test data, this rate is 0.451%. So, the results in the data are below seven per thousand. The graphical results showing these ratios are shown in Figure 13.

4. DISCUSSION AND CONCLUSION

In belt–pulley systems, the motion of the belt must be transmitted without any loss. There may be slippage between the belt and the pulley during moments of increased torque. The emergence of permanent elongation and loosening in the belt over time also necessitates tensioning systems.

In the present study, a group of pulleys consisting of different diameters was used as a tension pulley as an alternative to weighted or spring tension pulleys. By selecting the tension pulley with the most appropriate diameter based on the variable load and load distances, minimum slip values were achieved, and efforts were made to prevent shaft bearing strains along with the belt. Thus, both belt life and maintenance intervals will be extended.

In this study, two different artificial intelligence methods (GRNN, ANFIS) were preferred to estimate the main pulley rotations with variable motor speeds, variable weight amounts, variable center of gravity distances, and variable tension pulley diameters. Among these artificial intelligence methods, the GRNN method gave the best training and test results. For a 5% error, it achieved 100% success on training data and 77.78% success on test data. Also, for a 10% error, it achieved 100% success on training data and 87.78% success on test data. As seen in Table 6, according to R^2, RMSE, and MAE results, the GRNN network is more successful than the ANFIS network. In addition, the experimental results and GRNN conclusions are compared in Figure 14. It is observed that the GRNN network predicts values very close to the experimental results.

In future studies, different artificial intelligence methods will be tested with increased input parameters to increase the success of the model. In addition, more sensitive load transfers will be attempted with different belt structures.

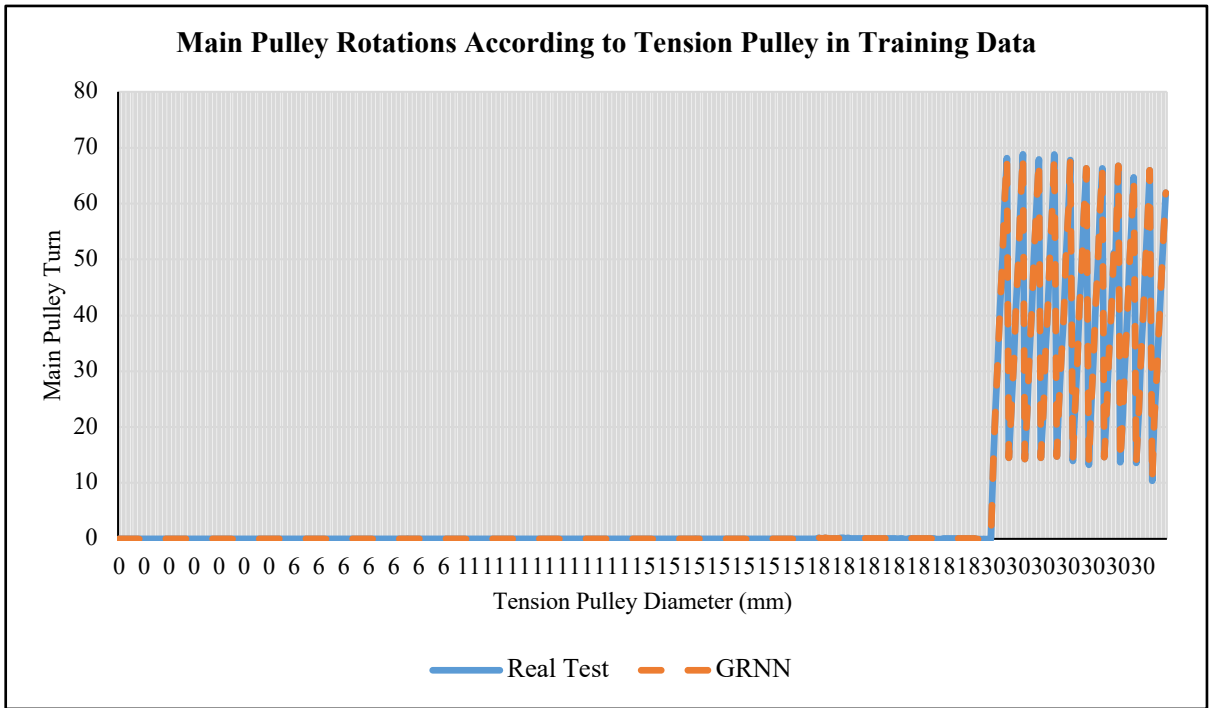

a)

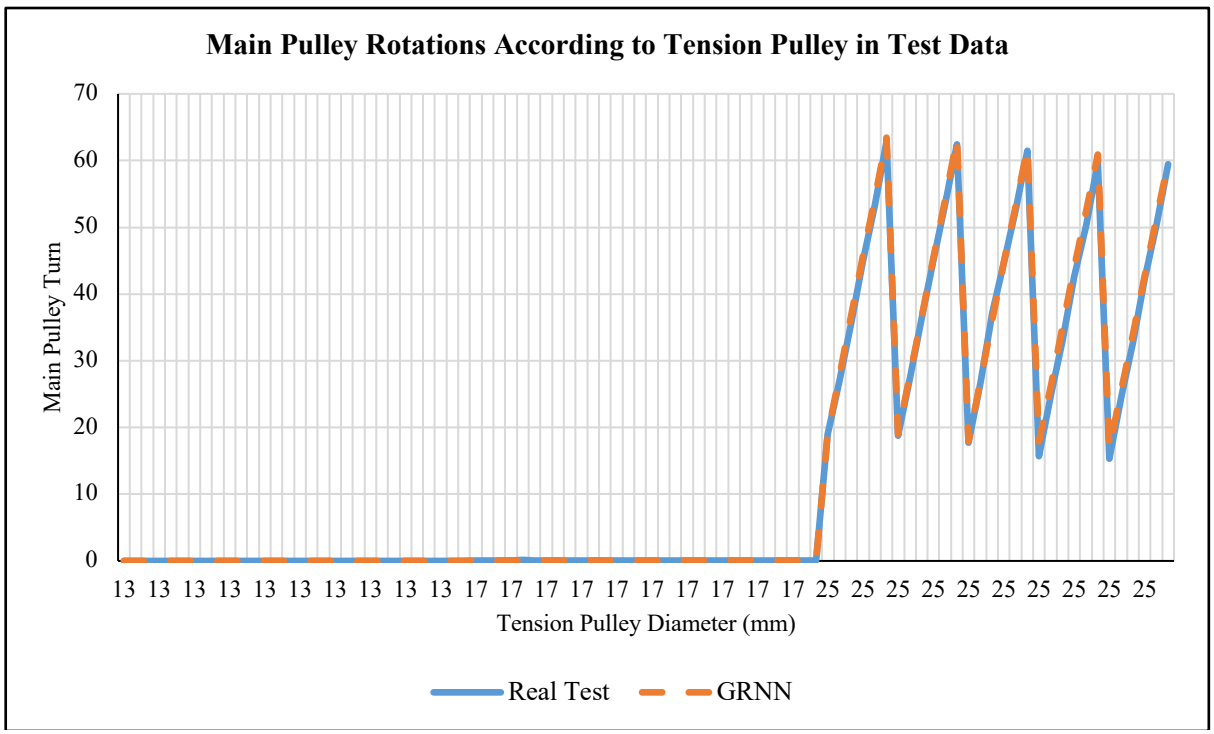

b)

Fig. 14. Main pulley rotations according to tension pulley diameter in a) Training data, b) Test data.

ACKNOWLEDGMENTS

The Scientific Research Projects Unit of Çukurova University supported the present work. Project Code: FBA-2023–16425.

REFERENCES

1. Kurbanoğlu, C 2009, *Makina Elemanları, Teori, Konstrüksiyon ve Problemler,* 2nd Ed, Nobel Yayın Dağıtım, Ankara.
2. Şekercioğlu, T 2017, *Makine Elemanları, Hesap Şekillendirme,* 3rd Ed, Birsen Yayınevi, İstanbul.
3. Ruan, S, Gao, S, Feng, J, Kong, Y, Han, Q & Chu, F 2024, 'Intelligent triboelectric V-belts with condition monitoring capability', *Mechanical Systems and Signal Processing*, vol. 209, pp. 111132.
4. Park, J, Park, Ji, Seo, HT, Liu, Y, Kim KS & Kim, S 2020, 'Control of tendon-driven (Twisted-string Actuator) robotic joint with adaptive variable-radius pulley', *20th International Conference on Control, Automation and Systems (ICCAS 2020),* BEXCO, Busan, Korea, pp. 1095-1098.
5. Ang, KK, Quek, C & Wahab, A 2002, 'MCMAC-CVT: a novel on-line associative memory-based CVT transmission control system', *Neural Networks*, vol. 15, pp. 219-236.
6. Müller, C & Schröder, D 2001, 'Modeling and Control of Continuously Variable Transmissions', *IFAC Advances in Automotive Control*, Karlsruhe, Germany, pp. 79-84.
7. Zhu, H, Zhu, WD & Fan, W 2021, 'Dynamic modeling, simulation and experiment of power transmission belt drives: A systematic review', *Journal of Sound and Vibration*, vol. 491, pp. 115759.
8. Cheng, G & Zu, JW 2003, 'Nonstick and stick-s1ip motion of a coulomb-damped belt drive system subjected to multi-frequency excitations', *ASME J. Appl. Mech.,* vol. 70, no. 6, pp. 871–884.
9. Hu, Y, Zhu, H, Zhu, WD, Li, C & Pi, Y 2017, 'Dynamic performance of a multi-ribbed belt based on an overlay constitutive model of carbon-black-filled rubber and experimental validation', *Mech. Syst. Signal Process.,* vol. 95, pp. 252–272.
10. Zhu, H, Hu, YM, Pi, YJ & Zhu, WD 2019, 'Hysteretic damping characteristics of a mechanical tensioner: Modeling and experimental investigation', *Proc. IMechE Part D J. Automob. Eng.,* vol. 233, no. 7, pp. 1890–1902.
11. di Napoli, M, Strähle, M, Ruzimov, S, Suarez Cabrera, LD, Amati, N & Tonoli, A 2016, 'Intelligent belt drive systems in hybrid powertrains: a multipurpose test rig', *IFAC-PapersOnLine*, Elsevier, vol. 49-21, pp. 047–053.
12. Feng, X, Shangguan, WB, Deng, JX, & Jing, XJ 2019, 'Modeling and dynamic analysis of accessory drive systems with integrated starter generator for micro-hybrid vehicles', *Proc. IMechE Part D J. Automob. Eng.,* vol. 233, no. 5, pp. 1162–1177.
13. Jung, JW, Lee, SH, Lee, GH, Hong, JP, Lee, DH & Kim, KN 2010, 'Reduction design of vibration and noise in IPMSM type integrated starter and generator for HEV', *IEEE Trans. Magnet.*, vol. 46, no. 6, pp. 2454–2457.
14. Balaji, R & Mockensturm, EM 2008, 'Dynamic analysis of a serpentine belt drive with a decoupler/isolator', *Int. J. Veh. Des.*, vol. 39, no. 3, pp. 208–231.
15. Ding, H, Zhen, Z & Chen, LQ 2018, 'Vibration reduction effect of one-way clutch on belt-drive systems', *Eur. J. Mech. - A/Solids*, vol. 71, pp. 378–385.
16. Martins, DR, & Pederiva, R 2013, 'Dynamic Analysis of a Serpentine Belt Drive with Automatic Tensioner', *22nd International Congress of Mechanical Engineering (COBEM 2013)*, Ribeirão Preto, SP, Brazil, pp. 2667-2675.

17. Bozacı, A 2005, *Makina Elemanları Cilt 2*, 1st Ed, Çağlayan Kitabevi, İstanbul.
18. Sağıroğlu, Ş, Beşdok, E & Erler, M 2003, *Mühendislikte Yapay Zeka Uygulamaları I, Yapay Sinir Ağları,* 1st Ed, Ufuk Yayıncılık, Kayseri.
19. Sahroni, A 2013, 'Design of Intelligent Control System Based on General Regression Neural Network Algorithm', *GSTF Journal on Computing (JoC)*, vol. 2, no. 4, pp. 103–110.
20. Türkşen, B 2015, *Dereceli (Bulanık) Sistem Modelleri*, 1st Ed, Abaküs Yayıncılık, İstanbul.
21. Baykal, N & Beyan, T 2004, *Bulanık Mantık, Uzman Sistemler ve Denetleyiciler*, 1st Ed, Bıçaklar Kitabevi, Ankara.
22. Pololu 2025, *4.4:1 Metal Gearmotor 25Dx60L mm HP 12V with 48 CPR Encoder (No End Cap)*, brushed DC motor, viewed 3 January 2025, <https://www.pololu.com/product/3213>.
23. Pololu 2025, *Pololu Simple High-Power Motor Controller 24v23*, motor controller card, viewed 3 January 2025, <https://www.pololu.com/product/1383>.
24. Humusoft 2025, *Humusoft*, data acquisition card, viewed 3 January 2025, <https://www.humusoft.cz/datacq/mf634/>.
25. Omron 2025, *Omron Industrial Automation*, encoder E6A2CW3C, viewed 3 January 2025, <https://www.ia.omron.com/product/item/2347/>.
26. Karunasingha, DSK 2022, 'Root Mean Square Error or Mean Absolute Error? Use Their Ratio as Well', *Information Sciences*, vol. 585, pp. 609–629.
27. Chicco, D, Warrens, MJ & Jurman, G 2021, 'The Coefficient of Determination R-Squared is More Informative than SMAPE, MAE, MAPE, MSE and RMSE in Regression Analysis Evaluation', *PeerJ Computer Science*, 7:e623, viewed 30 January 2025, <https://doi.org/10.7717/peerj-cs.623>.
28. Myttenaere, M, Golden, B, Grand, BL & Rossi, F 2016, 'Mean Absolute Percentage Error for Regression Models', *Neurocomputing*, vol. 192, pp. 38–48.